First-principles treatment of disorder effects in complex alloys: A study of $Ba_xK_{1-x}BiO_3$ and $BaPb_{1-x}Bi_xO_3$

A. Bansil and S. Kaprzyk*
Department of Physics, Northeastern University, Boston, Massachusetts 02115
(Received 17 December 1990)

We have developed a self-consistent Korringa-Kohn-Rostoker coherent-potential-approximation (KKR-CPA) approach to treat multiatom-per-unit-cell systems in order to study disorder effects in complex materials on a first-principles basis. Electronic structure of the high-T_c superconducting perovskites $Ba_xK_{1-x}BiO_3$ and $BaPb_{1-x}Bi_xO_3$ is discussed. KKR-CPA results for $x=0.1,0.2,\ldots,0.9$, as well as for the limiting single-impurity cases $x=0.0$ and $x=1.0$ are used to delineate rigid-band and non-rigid-band effects in the spectrum. McMillan-Hopfield parameters over the entire composition range are presented.

The electronic properties of complex materials have drawn an increasing interest in recent years. While reliable predictions of the electronic structures of ordered compounds with many atoms per unit cell have been obtained with use of the local-density approximation, a comparable description of the disordered phases has so far not been possible, even though wide variations in properties with various substitutions are commonly observed. The band theory of ordered phases is not suited for exploring a variety of phenomena in materials, and the need for generalizing the first-principles Korringa-Kohn-Rostoker coherent-potential-approximation (KKR-CPA) approach, which has already proven successful in simple binary alloys,[1-4] to treat complex systems is obvious.

With this motivation, we have developed the charge self-consistent KKR-CPA approach to treat disorder effects in complex materials on a first-principles basis; no free parameters other than the lattice data are involved. The theory is applied to the simple-cubic perovskites $Ba_xK_{1-x}BiO_3$ (Ba-K 1:1:3) and $BaPb_{1-x}Bi_xO_3$ (Pb-Bi 1:1:3). Ba-K 1:1:3 possesses a maximum T_c of 30 K for $x\approx 0.7$, while Pb-Bi 1:1:3 has a maximum T_c of 12 K for $x\approx 0.3$. Ba-K 1:1:3 is simple cubic, Pb-Bi 1:1:3 is slightly distorted tetragonal in the metallic range, but the presence of disorder is a feature of both the structures in the high-T_c composition region. These materials have been studied using the virtual-crystal-, rigid-band-, and supercell-type models, and also via the tight-binding CPA framework with parameters chosen to fit the band structures of the end compounds.[5-9] While these studies have yielded insight into the electronic structures of Ba-K 1:1:3 and Pb-Bi 1:1:3, we are unaware of any previous first-principles parameter-free study of these classic high-T_c superconductors. As the extensive experience with binary alloys shows, the simpler tight-binding CPA and rigid-band-type models cannot be expected to provide a realistic quantitative description of the disordered phases; if anything, these simpler models are likely to become generally less reliable as the complexity of the unit cell increases.

In connection with our formulation and implementation of the multicomponent KKR-CPA methodology, we note two points. First, we consider the full KKR-CPA Green's function, including terms which are real on the real-energy axis, even though such terms do not contribute to the density of states;[10] without the full KKR-CPA Green's function, we found it difficult to automate and carry out charge self-consistency cycles efficiently. Second, we have used the spectral representation of the KKR-CPA Green's function to implement a tetrahedron-type **k**-space integration method for disordered alloys. This approach yields orders of magnitude gains in efficiency and also allows us to treat the limiting cases of the single-impurity and the ordered compound with the same set of codes.

The specifics of the structural data and of the various convergence parameters used in the present work are as follows. The simple-cubic lattice constants used for $BaBiO_3$, $KBiO_3$, and $BaPbO_3$ are, 4.3485, 4.2886, and 4.2656 Å, respectively.[11,12] For intermediate compositions, lattice constants were obtained via Vegard's Law. The (Ba,K) muffin-tin radius was taken as $0.4571a(x)$, where $a(x)$ denotes the composition-dependent lattice constant. The radii for the Pb, Bi, and O atoms were taken to be the same, and were chosen so that the O atoms touch the Ba (or K) sphere. These procedures lead to a geometry very similar to that of Ref. 9 and yield a filling factor of approximately 0.66 in all cases.

Fully charge self-consistent KKR-CPA results were obtained in $Ba_xK_{1-x}BiO_3$ and $BaPb_{1-x}Bi_xO_3$ for 11 compositions $x=0.0,0.1,\ldots,1.0$ in each case; $x=0.0$ and 1.0 represent the case of a single impurity in the host. Calculations are semirelativistic with a von Barth–Hedin exchange-correlation potential; the core states were, however, treated relativistically. For most of the results shown in this paper, the maximum l cutoffs are $l_{\max}=2$ for Ba, K, Bi, and Pb sites, and $l_{\max}=1$ for O atoms. A number of self-consistent test runs were made using $l_{\max}=2$, and 3, respectively, for the O sites and the remaining sites, with little change in the results presented here, including the McMillan-Hopfield parameters.

Charge self-consistency cycles were carried out for each composition so that the maximum difference between the input and output potential on each atom was less than 5 mRy (the average difference was on the order of 2 mRy), and the maximum deviation in the total charge in each sphere was 0.003 electron. The Fermi-energy evaluation is accurate to about 3 mRy. The densities of states on the real axis are computed by using the tetrahedron method with 84 *ab initio* **k** points, which yield 216 tetrahedra in an irreducible $\frac{1}{48}$th wedge of the Brillouin zone. The charge self-consistency cycles in the complex plane employ 48 special points on an elliptical contour.[13] The accuracy of the final results with these parameters has been checked via additional computations in specific cases with 512 tetrahedra for real-energy density of state results, and 300 special points in the charge-density cycles for complex energies. The final KKR-CPA self-consistent potentials were reproduced to the quoted accuracies in several test cases from KKR-CPA codes on the real axis, and also from independent well-tested KKR codes in the case of perfect compounds.

Figure 1 displays the KKR band structure of $BaBiO_3$ for our self-consistent potential using $l_{max}=3$ for Ba and Bi, and $l_{max}=2$ for the O sites. The pattern and connectivity of our bands is similar to that of Ref. 9. Our Ba $5p$ band at an energy of -4 eV is about 0.5 eV lower than that of Ref. 9. The order of the Γ_{15} and Γ_1 levels around 2 eV (and other associated levels) depends sensitively on the position of the O $2p$ level, and differs between various calculations (see, e.g., Ref. 6). On the whole, the differences between Fig. 1 and other published results are comparable to those between various published band structures for $BaBiO_3$. Our computed band structures in $KBiO_3$ and $BaPbO_3$ (not shown) are similarly in reasonable accord with the corresponding published results.

The total KKR-CPA density of states in $Ba_xK_{1-x}BiO_3$ and $BaPb_{1-x}Bi_xO_3$ is presented in Fig. 2 for a representative set of compositions; as noted above, the computations were actually carried out for several compositions in addition to those shown in the figure. Figure 3 compares the density of states at the Fermi energy (E_F) in the alloys with the corresponding predictions of the rigid-band model based on the $BaBiO_3$ density of states. Figures 2 and 3 allow us to delineate the rigid-band as well as non-rigid-band changes in the spectrum of $BaBiO_3$ induced by (K for Ba) and (Pb for Bi) substitution.

Figure 2(a) shows that, for energies around the Fermi energy of $BaBiO_3$, the shape of the density of states curve is little affected by K-for-Ba substitution. In contrast, the Bi-for-Pb substitution, rapidly smooths the cusp at ≈ 0.6 Ry. This effect is related to the fact that the density of states around E_F in $BaBiO_3$ arises mainly from Bi and O sites, which are not influenced substantially when Ba is replaced by K; the Pb- and Bi-site densities, on the other hand, are quite different in this energy region, and thus lead to considerable changes upon alloying. Interestingly, the total density of states at E_F in both alloys (Fig. 3) is rather close to the predictions of a $BaBiO_3$-based rigid-band model. We see that the maximum difference between the rigid-band and the KKR-CPA results in the interesting composition range ($0.25 \le x \le 0.8$ in Fig. 3) is on the order of 16%; the deviations increase as the Fermi energy reaches the high density-of-states upper edge (at 0.4 Ry in Ba-K 1:1:3 and 0.5 Ry in Pb-Bi 1:1:3, Fig. 2) when approaching the $x=0$ limit. However, in view of the preceding observations, the agreement between the rigid-band and the KKR-CPA results in Fig. 3 in the case of Pb-Bi 1:1:3 should be considered fortuitous rather than of an intrinsic significance.

Turning to the energy region of 0.15–0.45 Ry, Fig. 2 shows that the shape of the density-of-states curve is quite similar in Ba-K 1:1:3 as well as Pb-Bi 1:1:3 for $0.3 \le E \le 0.45$ Ry in the upper part of the Bi $6s$–O $2p$ complex. For lower energies, $0.15 \le E \le 0.3$ Ry, we see substantial changes in the spectrum. For example, the largest peak at 0.29 Ry in $BaBiO_3$ splits and becomes less

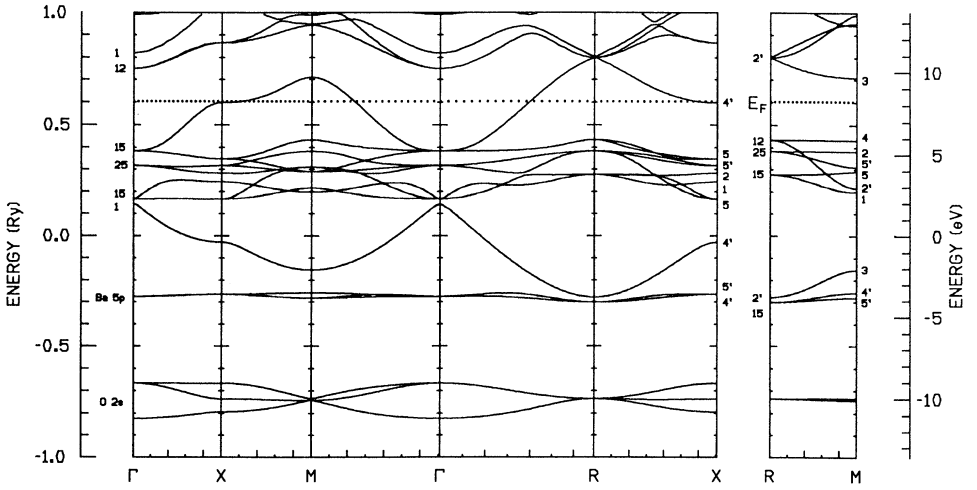

FIG. 1. Self-consistent KKR band structure of $BaBiO_3$.

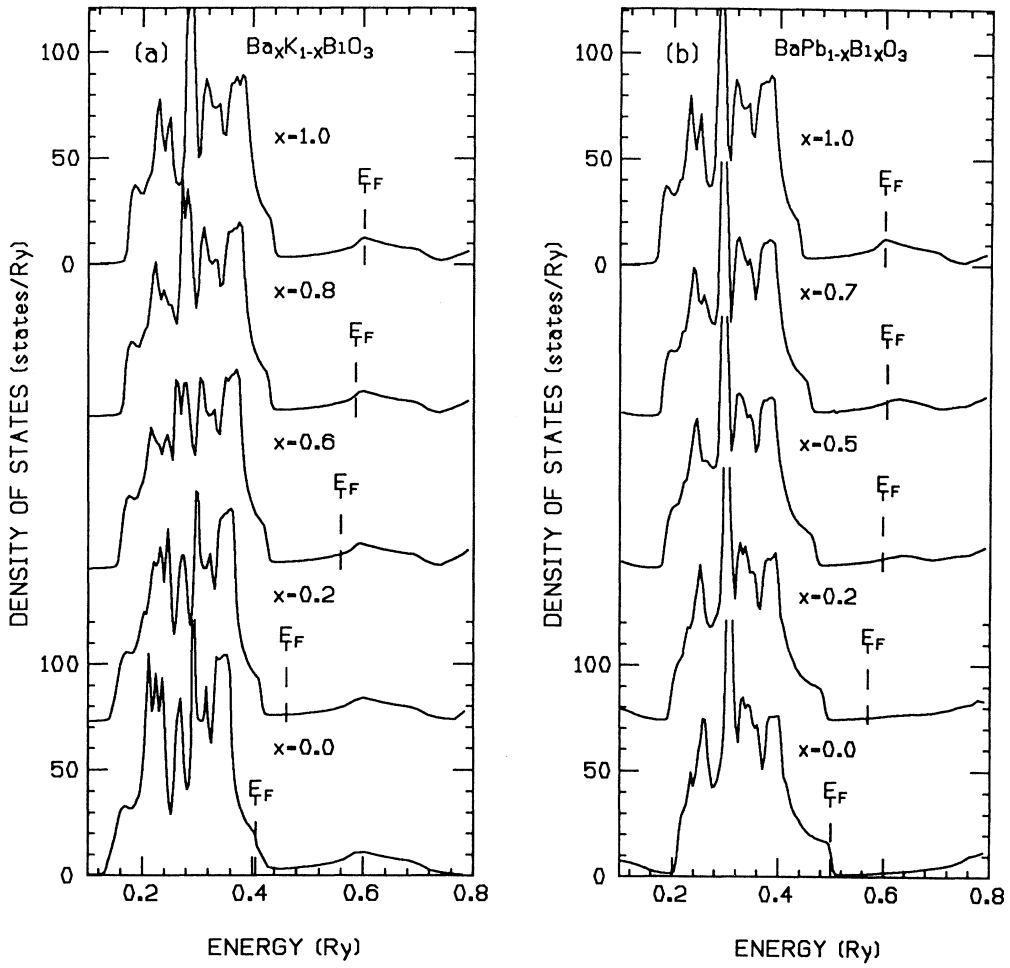

FIG. 2. Charge self-consistent KKR-CPA total densities of states in $Ba_xK_{1-x}BiO_3$ and $BaPb_{1-x}Bi_xO_3$. Fermi energies (E_F) are as marked.

prominent in Ba-K 1:1:3; in contrast, this peak is rather unaffected in Pb-Bi 1:1:3. The relative weights, positions, and shapes of the density-of-states peaks at 0.23 and 0.25 Ry in $BaBiO_3$ are influenced considerably in both Ba-K 1:1:3 and Pb-Bi 1:1:3. The preceding changes in the spectra between 0.15 and 0.3 Ry arise not only from changes in the component densities of states associated with the substituted sites, but also from the indirect changes induced on the O and other sites as a result of alloying.

We estimate the widths of the O $2p$ band in $BaBiO_3$, $Ba_{0.60}K_{0.40}BiO_3$, and $BaPb_{0.70}Bi_{0.30}O_3$ to be 3.55, 3.60, and 3.85 eV, respectively. There is thus an increase of about 0.3 eV in bandwidth in the Pb-Bi alloy case, but contrary to the conclusion of Ref. 9, there is hardly any increase in the Ba-K alloy. Also, in sharp distinction to the tight-binding model Hamiltonian study,[9] we find negligible density of states associated with the Ba or K sites at E_F in Ba-K 1:1:3, or with the Ba site in Pb-Bi 1:1:3.

We have computed the site-projected Hopfield parameters η within the rigid-muffin-tin approximation[14] using the relation

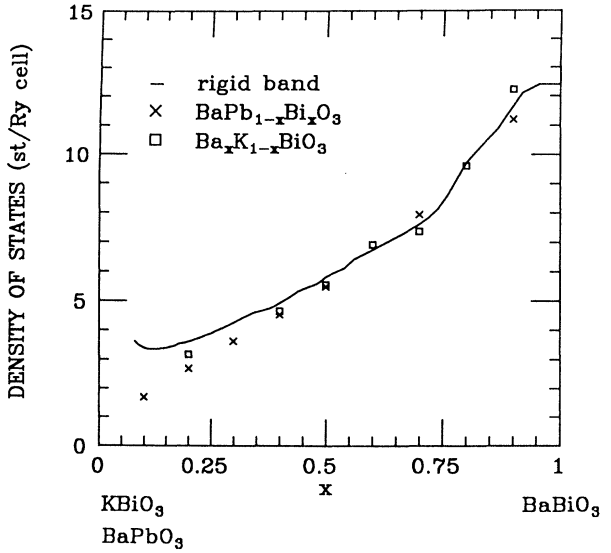

FIG. 3. Total density of states at the Fermi energy for the $BaBiO_3$-based rigid-band model, and the KKR-CPA results in $Ba_xK_{1-x}BiO_3$ and $BaPb_{1-x}Bi_xO_3$.

$$\eta=\sum_l \frac{(2l+2)N_l(E_F)N_{l+1}(E_F)}{(2l+1)(2l+3)N(E_F)} \left| \int_0^S dr\, r^2 R_l(r)\frac{dV}{dr}R_{l+1}(r) \right|^2 , \quad (1)$$

where $V(r)$ is the self-consistent KKR-CPA muffin-tin potential extending to the sphere radius S on the site in question, R_l are regular solutions of the Schrödinger equation normalized to unity in the sphere, N_l is the lth partial density on the site considered, and $N(E_F)$ is the total density of states at E_F. Figure 4 summarizes the results; the η values for the Ba and K sites in Ba-K 1:1:3 and for the Ba site in Pb-Bi 1:1:3 are negligibly small and are not shown. η_O increases with increasing x in $Ba_xK_{1-x}BiO_3$ and $BaPb_{1-x}Bi_xO_3$; η_{Bi}, however, increases with increasing potassium content x in $Ba_xK_{1-x}BiO_3$ but remains nearly flat over a wide range of bismuth content x in the $BaPb_{1-x}Bi_xO_3$ alloy in a non-rigid-band fashion. Our η values for $BaBiO_3$ are in good accord with those of Ref. 9. Based on the rigid-band model, Ref. 7, however, concludes that η_{Bi} is very small in $Ba_{0.71}K_{0.29}BiO_3$, while our computations [Fig. 4(a)] show that η_{Bi} is of same order as η_O (per O atom) in $Ba_{0.70}K_{0.30}BiO_3$. Figure 4(b) shows that η_O is smaller roughly by a factor of 2 in $BaPb_{0.70}Bi_{0.30}O_3$ compared to $Ba_{0.70}K_{0.30}BiO_3$, while η_{Bi} is hardly changed, suggesting that the O-mediated electron-phonon interaction may possess a lesser role while Bi plays a greater role in explaining the superconductivity of the Pb-Bi 1:1:3 system compared with the Ba-K 1:1:3 system. However, no firm conclusions can be reached in this regard, given the complexity of the relationship between the McMillan-Hopfield parameters and the transition temperatures and the approximations implicit in the form (1) for η.[15,16]

Some broader implications of this study deserve comment. Both Ba-K 1:1:3 and Pb-Bi 1:1:3 possess complex phase diagrams with many distortions of the basic cubic lattice and exhibit transitions to the nonmetallic (insulating or semiconducting) state.[11,12] In the superconducting range, only Ba-K 1:1:3 is perfectly cubic, Pb-Bi 1:1:3, as noted, is slightly distorted tetragonal. Since we find no great differences between the electronic structures of similarly doped cubic Ba-K 1:1:3 and Pb-Bi 1:1:3, our results imply, consistent with earlier work,[6,8,17] that structural distortions from the ideal cubic geometry (rather than substitutions) are important in explaining the metal-nonmetal transitions in these materials.

In summary, we have developed the first-principles self-consistent KKR-CPA approach for treating disorder phases in complex multicomponent alloys. Results for the simple-cubic perovskites $Ba_xK_{1-x}BiO_3$ and $BaPb_{1-x}Bi_xO_3$ over the whole composition range are presented. The density of states at E_F is found to be reasonably well described by the $BaBiO_3$-based rigid-band model. The shape of the underlying density of states around E_F is virtually unchanged, however, only in the case of $Ba_xK_{1-x}BiO_3$; in $BaPb_{1-x}Bi_xO_3$, the shape is

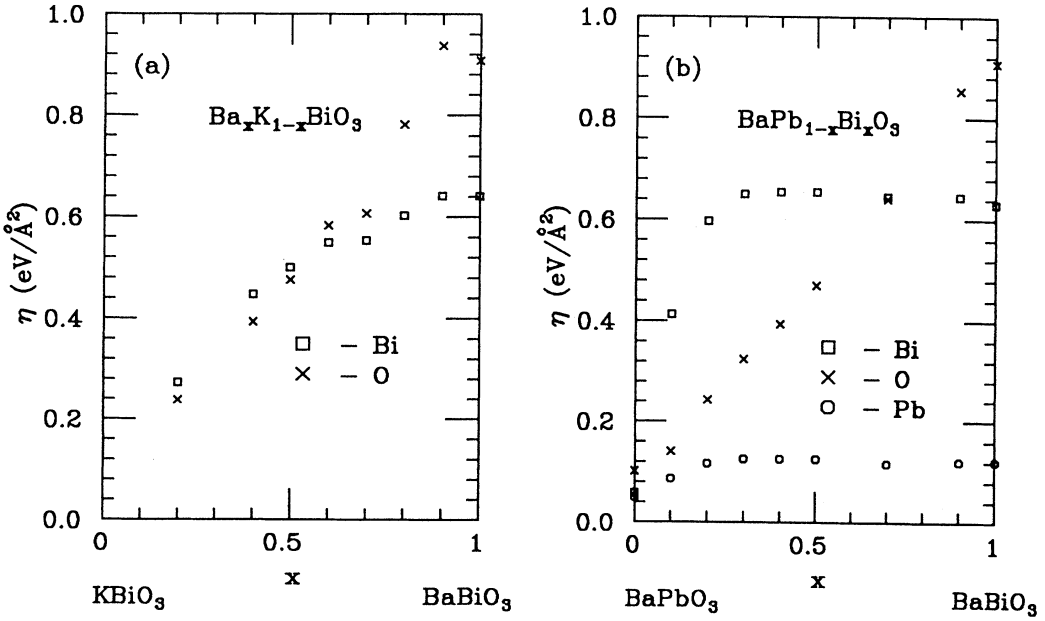

FIG. 4. McMillan-Hopfield parameters (η) in $Ba_xK_{1-x}BiO_3$ and $BaPb_{1-x}Bi_xO_3$ for various sites indicated in the legend.

changed substantially, and the aforementioned agreement should be considered fortuitous. Other rigid-band and non-rigid-band features in the density of states away from E_F are delineated; some conclusions based on the earlier virtual-crystal and tight-binding CPA models are similar to those of this study, while some others are not. The McMillan-Hopfield parameters for the various sites in both systems are evaluated over the entire composition range for the first time within the rigid-muffin-tin approximation; the computed behavior of η's indicates that, in a conventional electron-phonon mechanism of superconductivity, the coupling via the O sites in the Pb-Bi alloy may be substantially smaller compared to the Ba-K alloy in the superconducting range, while the Bi sites possibly play a more important role.

We acknowledge useful conversations with R. Benedek. This project was supported by the Department of Energy (DOE) Grant No. 85 ER45223, and benefitted from the allocation of supercomputer time on the Energy Research Cray Y-MP8/864 computer at Lawrence Livermore National Laboratory (LLNL), and the San Diego Supercomputer Center, and a travel grant from the Polish Academy of Sciences Program No. CPBP 01.12.

*Permanent address: Academy of Mining and Metallurgy, Institute of Physics and Nuclear Techniques, Krakow, Poland.

[1]A. Bansil, in *Electronic Band Structure and its Applications,* Vol. 283 of *Lecture Note Series,* edited by M. Yussouff (Springer-Verlag, Heidelberg, 1987), p. 273.

[2]H. Ehrenreich and L. M. Schwartz, in *Solid State Physics,* edited by H. Ehrenreich, F. Seitz, and D. Turnbull (Academic, New York, 1976), Vol. 31.

[3]G. M. Stocks and H. Winter, in *Electronic Structure of Complex Systems,* edited by P. Phariseau and W. Temmerman (Plenum, New York, 1984).

[4]See J. Kudrnovský, V. Drchal, M. Šob, N. E. Christensen, and O. K. Andersen, Phys. Rev. B **40**, 10029 (1989), and references therein, for work applying CPA within the linear muffin-tin orbital (LMTO) framework to disordered alloys. For an extensive discussion of literature, including some early non-self-consistent KKR-CPA computations on relatively simple, two-atom-per-unit-cell hydrides, see Ref. 1–3 above.

[5]L. F. Mattheiss and D. R. Hamann, Phys. Rev. Lett. **60**, 2681 (1988).

[6]L. F. Mattheiss and D. R. Hamann, Phys. Rev. B **28**, 4227 (1983).

[7]N. Hamada, S. Massidda, A. J. Freeman, and J. Redinger, Phys. Rev. B **40**, 4442 (1989).

[8]K. Takegahara and T. Kasuya, J. Phys. Soc. Jpn. **56**, 1478 (1987).

[9]D. A. Papaconstantopoulos, A. Pasturel, J. P. Julien, and F. Cyrot-Lackmann, Phys. Rev. B **40**, 8844 (1989).

[10]Specifically, the (r,r) matrix element of the KKR-CPA Green's function contains the term $\sum_L Y_L(\hat{\mathbf{r}})Z_l^i(r_<)J_l^i(r_>)Y_L(\hat{\mathbf{r}})$, averaged over the sites i, where Z_l^i and J_l^i are the regular and irregular solutions of the radial Schrödinger equation, respectively in the ith muffin-tin sphere. This term, which is real for real energies, is included in our computations for real as well as complex energies.

[11]S. Pei, J. D. Jorgensen, B. Dabrowski, D. G. Hinks, D. R. Richards, A. W. Mitchell, J. M. Newsam, S. K. Sinha, D. Vaknin, and A. J. Jacobson, Phys. Rev. B **41**, 4126 (1990).

[12]D. E. Cox and A. W. Sleight, Solid State Commun. **19**, 969 (1976); Acta Crystallogr. B **35**, 1 (1979).

[13]One charge self-consistency cycle (including the necessary KKR-CPA solutions) with 48 points on the complex energy contour took approximately 4 min CPU time on the Cray Y-MP8/864 computer.

[14]G. D. Gaspari and B. L. Gyorffy, Phys. Rev. Lett. **29**, 801 (1972).

[15]Notably, the composition dependence of η_O as well as η_{Bi} in Fig. 4 is rather similar to the measured composition dependence of T_c in Ba-K 1:1:3. Shirai *et al.* (Ref. 16) obtain a reasonable agreement with measured T_c's in Ba-K 1:1:3 using the conventional electron-phonon mechanism.

[16]M. Shirai, N. Suzuki, and K. Motizuki, J. Phys.: Condens. Matter **2**, 3553 (1990).

[17]W. Weber, Jpn. J. Appl. Phys. **26**, 981 (1987).